Dynamics of subduction and plate motion in laboratory experiments : insights into the "plate tectonics" behavior of the Earth

Nicolas Bellahsen, C. Faccenna, F. Funiciello

Dynamics of subduction and plate motion in laboratory experiments: Insights into the "plate tectonics" behavior of the Earth

Nicolas Bellahsen,[1] Claudio Faccenna, and Francesca Funiciello
Dipartimento di Scienze Geologiche, Università degli Studi Roma TRE, Rome, Italy

Received 28 January 2004; revised 23 September 2004; accepted 20 October 2004; published 6 January 2005.

[1] Three-dimensional laboratory experiments have been designed to investigate the way slab-bearing plates move during subduction inside the mantle. In our experiments a viscous plate of silicone (lithosphere) subducts under its negative buoyancy in a viscous layer of pure honey (mantle). Varying thickness, width, viscosity, and density of the plate and mantle, three characteristic modes of subduction are observed: a retreating trench mode (mode I), a retreating trench mode following a transient period of advancing trench (mode II), and an advancing trench mode (mode III). These modes are characterized by different partitioning of the amount of subduction into plate and trench motion. Our experiments show that the velocity of subduction can be modeled by the dynamic interaction between acting and resisting forces, where lithospheric bending represents 75–95% of the total resisting forces. However, our experimental results also show the impossibility to predict a priori the plate velocity only from the velocity of subduction without considering trench migrations. We find experimentally that the lithospheric radius of curvature, which depends upon plate characteristics (stiffness and thickness) and the mantle thickness, exerts a primary control on the trench behavior. Our results suggest that the complexity of the style of subduction could be controlled by geometrical rules of a plate bending inside a stratified mantle. The Earth system is in the crucial range for the interplay between the rigidity of the plate and the mantle stratification: this setting may be the responsible for the complexity of the past and present tectonic styles.

Citation: Bellahsen, N., C. Faccenna, and F. Funiciello (2005), Dynamics of subduction and plate motion in laboratory experiments: Insights into the ''plate tectonics'' behavior of the Earth, *J. Geophys. Res.*, *110*, B01401, doi:10.1029/2004JB002999.

1. Introduction

[2] On the Earth's surface, plates move at different rates. The slab-bearing plates usually are the fastest, attaining rates of up to 10 cm yr^{-1}. However, in the past, plate velocities and directions changed rather abruptly. Subduction zones, where plates bend to enter into the Earth's mantle, are also nonstationary. They move and have moved intermittently, showing episodes of fast motion punctuated by episodes of stasis. Actually, all of the tectonic processes recorded on the Earth, from the opening of back-arc basins to the building of orogens, reveal that plates and trenches changed direction and speed of motion during time. The variety of tectonic styles on the surface of the Earth is impressive as some trenches advance toward the overriding plate while some others retreat and subducting slabs show a wide range of possible shapes and geometries. In particular, the actual motion of the Earth's trenches is equally partitioned between trenches that advance and trenches that retreat [*Heuret and Lallemand*, 2004].

[3] Geodynamic models are able to predict the present and past velocity field of the plates. These models are based on the idea that plate motion is driven by the negative thermal buoyancy of the subducting lithosphere slab pull [*Forsyth and Uyeda*, 1975; *Chapple and Tullis*, 1977; *Becker and O'Connell*, 2001] or by the mantle flow excited by the downwelling of thermal anomalies [*Conrad and Lithgow-Bertelloni*, 2002] and is resisted either by the strength of the lithosphere (i.e., bending) [*Becker et al.*, 1999; *Conrad and Hager*, 1999] or by viscous shear stress in the mantle [*Turcotte and Oxburgh*, 1967] or by a combination of both [*Becker and O'Connell*, 2001; *Conrad and Lithgow-Bertelloni*, 2002]. These computations indicate the way mantle convection works driving plates but suffer from imposed kinematic conditions for the slab-trench system. For example, models designed in a way that plates and trenches can move accordingly to slab dynamics reveal that the interaction between slab and mantle is far from simple and that the resulting velocity field of the plate-trench system is variable and nonsteady [e.g., *Zhong and*

[1]Now at Department of Geological and Environmental Sciences, Stanford University, Stanford, California, USA.

0148-0227/05/2004JB002999$09.00

Gurnis, 1995]. These simulations show that the assumption of plates moving at the same rate as the subducting slabs is not always pertinent.

[4] Here, we present the results of a complete set of three-dimensional (3-D) laboratory experiments where a thin viscoelastic sheet of silicone putty subducts under its own weight in the middle of larger tank filled with a viscous solution of glucose syrup driving the attached plate. We tested the role of different parameters (plate thickness, viscosity, density, and width and mantle thickness) in controlling the style of subduction and we found that it is mainly controlled by the way the slab bends at the trench. Our models present the advantage of being three-dimensional with the trench kinematics controlled only by slab dynamics, and the disadvantages of having a rather simple rheological layering for the lithosphere and a lack of temperature-dependent viscosity. We have found that the slab can subduct into the mantle attaining different styles and kinematics. We have identified two parameters that control the style of subduction and in turn the plate motion: the radius of curvature of the subducting plate and the width of the plates. In particular, when the radius of curvature is approximately equal to half of the thickness of the upper convecting mantle, the slab-trench-plate kinematics is able to simulate the variety of styles observed in plate tectonics. In these conditions, the plate-slab system is also sensible to the variation of the size of the plate.

2. Model Setup

2.1. Model Definition

[5] Our experiments were setup in the following framework: (1) viscous rheology, (2) no external forces, (3) passive convective mantle, (4) isothermal system, (5) impermeable bottom to the mantle, and (6) no overriding plate. A more detailed explanation of these laboratory assumptions is noted below.

[6] 1. In this work, we have followed the experimental choice adopted by previous authors [*Kincaid and Olson*, 1987; *Griffiths et al.*, 1995; *Guillou-Frottier et al.*, 1995; *Faccenna et al.*, 1996; *Becker et al.*, 1999; *Faccenna et al.*, 1999; *Funiciello et al.*, 2003] as described further. In addition, we further simplified the slab rheology using a linearly viscous material whereas laboratory experiments show that natural materials follow to a creep power law of deformation [*Brace and Kohlstedt*, 1980]. As a Newtonian material has a stronger response to deformation than a power law fluid [*Ranalli*, 1995], the velocities observed in laboratory should be considered as a lower bound.

[7] 2. Only the slab pull force was driving the entire process. No external boundary conditions such as plate or trench velocity were applied.

[8] 3. We were interested in isolating the effect of advection inside the mantle produced by the subducting slab. Flow was only generated by subduction and we did not consider the effect of global [*Hager and O'Connell*, 1978; *Ricard et al.*, 1991] or local background flow that was not generated by the subducting slab.

[9] 4. We neglected thermal effects during the subduction process. Hence the temperature profile of the model was translated into chemical density contrast, staying constant throughout the experiment despite the role of thermal diffusion and phase changes [*Bunge et al.*, 1997; *Lithgow-Bertelloni and Richards*, 1998; *Tetzlaff and Schmeling*, 2000]. This situation is equivalent to quasi-adiabatic conditions. As the velocity of the subduction process was much higher than 1 cm yr^{-1}, we could neglect temperature changes during subduction [*Wortel*, 1982; *Bunge et al.*, 1997].

[10] 5. The bottom of the box was assumed to be an impermeable barrier for flow, such as, for example, the 660 km discontinuity. The validity of this assumption is motivated by previous studies, which found that the direct penetration of the slab through the transition zone is inhibited if the timescale of the analyzed process is limited (order of few tens of million years) and if the viscosity increase in the lower mantle is at least of an order of magnitude [*Davies*, 1995; *Guillou-Frottier et al.*, 1995; *Christensen*, 1996; *Funiciello et al.*, 2003].

[11] 6. The overriding plate was not modeled. Hence we assumed that the plate boundary is weak since it has the viscosity of the upper mantle. *Conrad and Hager* [1999] suggested that the overriding and subducting plate interaction might not be energetically important. However, *Conrad et al.* [2004] suggested that the overriding plate might exert some stresses on the subducting plate. Here, we assumed that the overriding plate passively moves with the retreating trench. This choice is able to influence the rate of the subduction process but not its general behavior [*King and Hager*, 1990].

2.2. Materials

[12] The subduction framework (Figure 1a) was approximated by a linear viscous multilayer system [*Kincaid and Olson*, 1987; *Griffiths et al.*, 1995; *Guillou-Frottier et al.*, 1995; *Faccenna et al.*, 1996; *Becker et al.*, 1999]. In particular, we selected silicone putty (Rhodorsil Gomme, PBDMS + galena fillers) and pure honey to approximate the long-term behavior of the lithosphere/upper mantle system. Silicone putty is a viscoelastic material that, at experimental strain rates, behaves only viscously [*Weijermars and Schmeling*, 1986] as the experimental timescale is higher than the Maxwell relaxation time (about 1 s). The upper mantle was modeled by honey, which is a Newtonian low-viscosity and high-density fluid.

[13] Physical parameters used to scale our laboratory models are listed in Table 1. Scale factor for length is 1.6×10^{-7} (1 cm in the experiment correspond to 60 km). The scale density factor between the oceanic lithosphere and the upper mantle is 1.07 whereas the viscosity ratio between the slab (η_l) and the upper mantle (η_m) is fixed to 3000 respecting the range of natural viscosity contrast [*Hager*, 1984; *Davies and Richards*, 1992; *Mitrovica and Forte*, 1997]. Considering the imposed scale ratio for length, gravity, viscosity, and density (Table 1), we calculated that 1 min in the model corresponds to about 1 Myr in nature.

2.3. Experimental Procedure

[14] The multilayered system was arranged in a square Plexiglas tank (Figure 1a) (20 cm high, 80 cm long, and 80 cm wide). The plate was free to move, responding self consistently to subduction dynamics. Therefore we assumed that plates were completely surrounded by fault zones

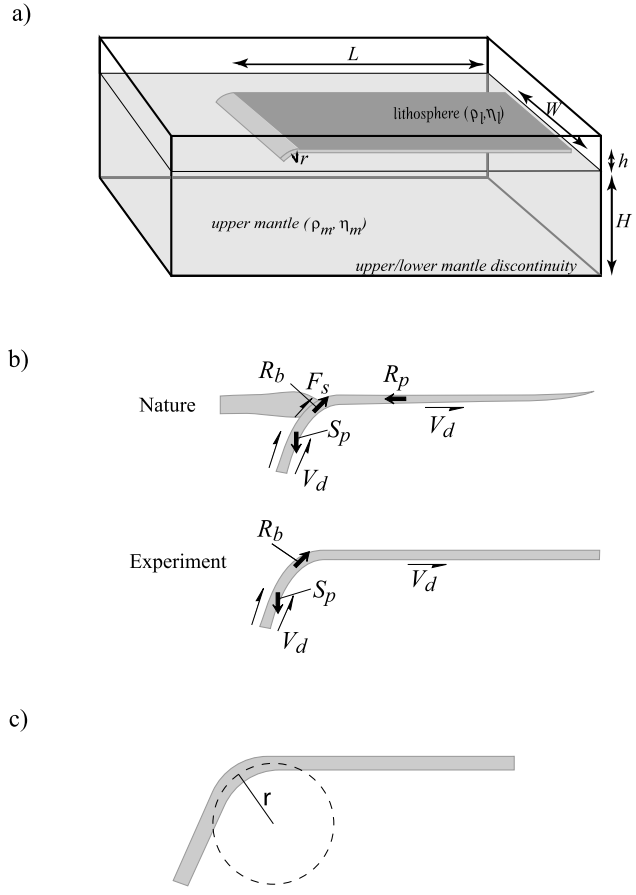

Figure 1. Experimental setup. (a) Experimental box. The lithosphere is simulated by means of a silicone plate of density ρ_l, viscosity η_l, width w, thickness h, and length L. The mantle is simulated by means of honey of density ρ_m, viscosity η_m, and thickness H. (b) Forces at work in the subduction factory and in the simplified experimental setting. (c) Method used to measure the radius of curvature. We adjusted a circle to the upper bent area to fit the slab curvature.

(trench and transform faults) whose equivalent viscosity is that of the upper mantle. These conditions resulted in a faster velocity [*King and Hager*, 1990] but ensured the maximum mobility of the plate.

[15] Experiments were designed as a parameter-searching test to analyze the role of factors controlling plate and trench motion of a subducting plate. This systematic study has been carried out by widely changing geometrical and rheological parameters of the system and testing their relative influence on the kinematics of subduction. A total number of 31 (out of a set of 60) different experiments are detailed here and were performed using variable combinations of thickness, viscosities and densities of the plate and mantle (Table 2). Viscosity and density of the silicone putty were varied by mixing the pure silicone putty with variable amount of galena fillers. Experiments were performed at least twice to ensure reproducibility.

[16] Each experiment was monitored using a sequence of photographs taken in time intervals in the lateral and top view. Trench retreat, plate motion, amount of subduction and dip of the slab were measured using image-processing tools. From these measurements, diagrams of the amount of trench and plate motion and amount of subduction versus time were constructed. In addition, the steady state subduction velocity was calculated during the last (steady state) phase of each subduction experiment. During this steady state phase, we measured the radius of curvature of the subducting plate (Figure 1c).

[17] In the initial configuration, the leading edge of the silicone plate was forced downward to a depth of 3 cm (corresponding to about 200 km in nature) inside the pure honey as a means of starting the subduction process.

3. Forces at Work

[18] *Conrad and Hager* [1999] proposed an analytical solution for the plate velocity in a 2-D context of subduction with a fixed trench. In this case, the plate and subduction velocities are equal. However, in our experiments, the trench moves as a response of the mode of subduction. Thus the plate and subduction velocities became unequal. We adopted the *Conrad and Hager* [1999] formulation as an analytical solution for the subduction velocity and not

Table 1. Scaling of Parameters in Nature and in Laboratory for a Reference Experiment

Parameter	Nature	Reference Model
g, gravitational acceleration, m s^{-2}	9.81	9.81
Thickness, m		
h, oceanic lithosphere	70,000	0.012
H, upper mantle	660,000	0.11
Scale factor for length L_{model}/L_{nature}	1.6×10^{-7}	
Density, kg m^{-3}		
ρ_l, Oceanic lithosphere	3,300	1482
ρ_m, upper mantle	3,220	1383
Density contrast (ρ_l-ρ_m)	80	99
Density ratio (ρ_l/ρ_m)	1.025	1.072
Viscosity, Pa s		
η_l, oceanic lithosphere	10^{22}–10^{23}	1.6×10^5
η_m, upper mantle	10^{20}–10^{21}	100
Viscosity ratio ($\eta' = \eta_l/\eta_m$)	10–10^3	$\sim 10^3$
t, characteristic time, s	3.1×10^{13}	60
$(t_{nature}/t_{model} = (\eta_n/\eta_m)/(\sigma_n/\sigma_m) = (\eta_n/\eta_m)/[(\Delta\rho g l)_n/(\Delta\rho GL)_m])$	(1 Myr)	(1 min)

Table 2. Description of Materials and Parameters Used in the Selected Experiments

Experiment	H, m	$\Delta\rho$, kg m^{-3}	w, m	h, m	r, m	η_l, Pa s	Mode of Subduction
1	0.11	100	0.1	0.006	0.03	3.6E + 05[a]	III
2	0.11	100	0.1	0.009	0.045	3.6E + 05	III
3	0.11	100	0.1	0.012	0.055	3.6E + 05	I
4	0.11	100	0.1	0.017	0.08	3.6E + 05	I
5	0.11	100	0.05	0.012	0.045	2.0E + 05	III
6	0.11	100	0.05	0.012	0.045	2.0E + 05	III
7	0.11	100	0.05	0.012	0.045	2.0E + 05	III
8	0.11	100	0.1	0.012	0.045	2.0E + 05	III
9	0.11	100	0.1	0.012	0.045	2.0E + 05	III
10	0.11	100	0.15	0.012	0.045	2.0E + 05	II
11	0.11	100	0.18	0.012	0.045	2.0E + 05	II
12	0.11	100	0.22	0.012	0.045	2.0E + 05	II
13	0.11	100	0.27	0.012	0.045	2.0E + 05	II
14	0.11	100	0.32	0.012	0.045	2.0E + 05	II
15	0.11	100	0.39	0.012	0.045	2.0E + 05	III
16	0.11	100	0.27	0.009	0.045	3.6E + 05	III
17	0.11	100	0.36	0.009	0.045	3.6E + 05	III
18	0.11	100	0.2	0.006	0.03	3.6E + 05	III
19	0.11	100	0.3	0.006	0.03	3.6E + 05	III
20	0.11	100	0.5	0.006	0.03	3.6E + 05	III
21	0.11	100	0.6	0.006	0.03	3.6E + 05	III
22	0.11	150	0.1	0.012	0.055	1.2E + 05	I
23	0.11	150	0.19	0.012	0.055	1.2E + 05	I
24	0.11	150	0.3	0.012	0.055	1.2E + 05	I
25	0.16	100	0.05	0.012	0.045	2.0E + 05	II
26	0.16	100	0.1	0.012	0.045	2.0E + 05	II
27	0.16	100	0.1	0.012	0.045	2.0E + 05	II
28	0.16	100	0.15	0.012	0.045	2.0E + 05	II
29	0.16	100	0.35	0.012	0.045	2.0E + 05	II
30	0.11	100	0.3	0.012	0.07	5.0E + 05	I
31	0.06	100	0.1	0.012	0.045	2.0E + 05	III

[a]Read 3.6E + 05 as 3.6×10^5.

the plate velocity. The subduction velocity (v_s) can be predicted using

$$v_s = \left[C_s \Delta\rho g z h - C_f \tau l\right] \Big/ \left[2C_l \eta_l (h/r)^3 + 3\eta_m (A + C_m)\right] \quad (1)$$

where C_s, C_f, C_l, and C_m are constants for slab pull, shear at subduction fault, lithospheric bending, and mantle contribution, respectively; $\Delta\rho$ is the density contrast between the slab and the mantle; g is the gravity acceleration; z is the depth of the slab; h is the plate thickness; l is the length of the subduction fault; η_l and η_m are the viscosity of the lithosphere and the mantle, respectively; τ is the shear stress generated at the subduction fault; and r is the radius of curvature. The ridge push R_p is here neglected as considered as one order of magnitude lower than the slab pull S_p (Figure 1b). The velocity of subduction here results from the equilibrium between the active or driving force related to the gravitational force (slab pull, S_p) and resisting forces (resistance at subduction fault zone F_s, viscous dissipation at trench due to lithospheric bending R_b and along the slab sides due mantle viscous shear V_d) (Figure 1b). *Conrad and Hager* [1999] suggested that the subducting and overriding plate interaction may not be energetically important. Thus, in our experiments, we assumed that the subduction fault zone has the same viscosity as the upper mantle. Hence, in the force balancing, the resistance to sliding along this weak subduction fault is one order of magnitude less than the other resisting forces and can be neglected.

[19] Equation (1) has been used to calculate a predicted subduction velocity that will be compared to the observed velocities. In the following, each force is described and the way we calculated the constants is explained. *Conrad and Hager* [1999] give the analytical solution for a 2-D context. Here, we adapted it to a 3-D context.

3.1. Driving Force

[20] The driving force of our experiments is the negative buoyancy of the subducting plate (S_p, Figure 1b). The total rate of potential energy release once the slab has reached the bottom of the box scales as

$$\Phi_{sp} = C_s \Delta\rho g h H v_s \quad (2)$$

[21] For the case of retreating slab the value of h is replaced by "$h \sin \alpha$," where α is the value of the dip of the slab. In this way, we take into account the influence of the shallower slab dip.

3.2. Resisting Forces

[22] The energy dissipated at the trench due to bending (R_b, Figure 1b) has been previously analyzed by means of numerical and laboratory experiments [*Conrad and Hager*, 1999; *Becker et al.*, 1999; *Funiciello et al.*, 2003]. The lithospheric viscous dissipation at trench is proportional to [*Turcotte and Schubert*, 1982]:

$$\Phi_b = 2C_l \eta_l v_s^2 (h/r)^3 \quad (3)$$

[23] For our linear viscous slab model, the same relationship holds when the slab bends at the 660 km discontinuity since the bending geometry is roughly the same at depth. Its contribution should then be doubled if integrated over the whole slab. The value of the radius of curvature, r, is fundamental; it is found to be variable during the experiments, as it is strongly dependent on the dip of the slab, its viscosity and thickness. However, a constant value can be observed during the last steady state stage of subduction and that value is used. The radius of curvature is thus measured at trench and has a similar value at depth when the slab bends along the bottom of the box. In nature, this radius of curvature (at depth) may be decreased due to the temperature increase. This phenomenon is neglected in our experiments.

[24] The energy dissipated by viscous resistance exerted on the slab and on the plate (V_d, Figure 1b) has been evaluated here both analytically and experimentally. It is derived from *Turcotte and Schubert* [1982] and *Conrad and Hager* [1999] and it is generally expressed as

$$\Phi_m = 3\eta_m v_s^2 (A + C_m) \quad (4)$$

where A is the aspect ratio of the convective cell and C_m depends upon the streamline geometry. For the case of $L > z$, A is proportional to L/H, where L is the length of the subducting bearing plate and H the mantle thickness. In order to take into account the influence of the third dimension, we consider the effective plate length L_{eff} as

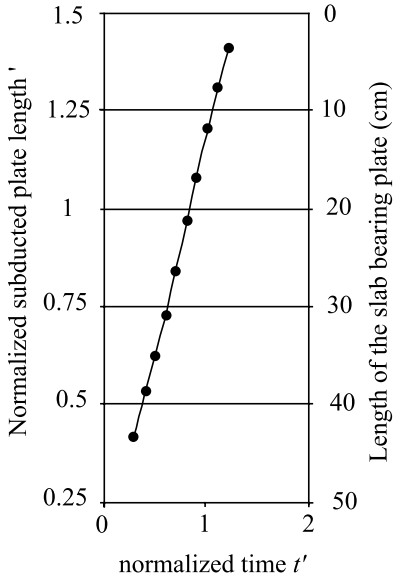

Figure 2. Diagram of the normalized subducted plate length and length of slab-bearing plate versus normalized time. Only the last steady state phase is represented and shows that the subduction velocity does not depend on the plate length. The plate was originally 70 cm long. The normalized time t' is calculated from the beginning of the steady state phase.

the square root of the plate/slab area subjected to shear drag as:

$$L_{\text{eff}} = 2(HW)^{1/2} + (WL)^{1/2} \tag{5}$$

where the first member defines the slab contribution and the other the plate contribution. W is the width of the plate (Figure 1). Hence equation (4) becomes

$$\Phi_m = 3\eta_m v_s^2 \left\{ C_m + \left[2(HW)^{1/2} + (WL)^{1/2} \right] / H \right\} \tag{6}$$

Of course, equation (6) represents a first-order evaluation of the resistance. In our system, for example, the length of the plate decreases during subduction. This decrease does not produce any changes of the velocity of subduction (Figure 2). This effect seems then very small. *Conrad and Hager* [1999] estimated that at least 30% of the energy dissipated in the upper mantle is related to the viscous coupling between the plate and the mantle. In our experiments, the mantle contribution includes a twofold effect. One is related to the viscous coupling between plate and mantle and the other is related to the 3-D configuration as the trench migration generate overpressure and, in turn, flow around the slab edges.

3.3. Analytical Solution and Constants

[25] The analytical solution we used to calculate the subduction velocity can then be rewriting as

$$v_s = C_s \Delta\rho g z h / \left\{ 2C_l \eta_l (h/r)^3 + 3\eta_m \left[C_m + \left(2(HW)^{1/2} + (WL)^{1/2} \right) / H \right] \right\} \tag{7}$$

[26] The evaluation of the contribution of each component can be done by establishing the value of the constants for slab pull (C_s), lithospheric (C_l) and mantle resistance (C_m). These constants have been estimated using our experimental results. We obtained the value of 0.9 for the ratio between the slab pull and the bending constants (C_s/C_l). This value has been found removing at first the dependency of the subduction velocity from the width of the plate. It has been done drawing the regression line (see section 4.4) and identifying the characteristic velocity of subduction for ideal 2-D cases. Hence we found the best fit to the subduction velocity of these 2-D cases with the contribution of only equations (2) (slab pull) and (3) (bending) obtaining the value of 0.9. Assuming a value in the order of unity for the slab pull constant, C_s, the bending constant, C_l, is then of 1.1. The constant for the mantle contribution (C_m) has been evaluated in the order of 2 by fitting the subduction velocity for the cases of plate with different widths (see section 4.4).

3.4. Scaling and Nondimensionalization

[27] Lithosphere viscosity can be nondimensionalized by mantle viscosity $\eta' = \eta_l/\eta_m$. The width of the plate is normalized for the depth of mantle giving an aspect ratio $w' = W/H$. The thickness of the plate can be normalized for the thickness of the mantle $h' = h/H$. The thickness of the mantle can be normalized for the plate thickness $H' = H/h$. The velocity can be normalized for a typical velocity $v_s' = V_s/(\Delta\rho g H h/\eta_m)$. This velocity is calculated for a reference slab taking a characteristic mantle thickness of 0.11 m (corresponding to 660 km in nature) and a characteristic plate thickness of 0.012 m (corresponding to 70 km in nature). The time is normalized by the time necessary for the reference slab to reach the 660 km discontinuity (t'). This characteristic time, t', is calculated using the formula of *Becker et al.* [1999], *Conrad and Hager* [1999], and *Faccenna et al.* [2001]. They show that the slab tip depth can be related to the initial slab depth and exponentially to the time. The time necessary to reach the 660 km discontinuity can then be expressed as

$$t' = \ln(H/z_0) \times h^2 \times \eta_l / \left(\Delta\rho g r^3 \right) \tag{8}$$

where z_0 is the initial slab tip depth, H is the upper mantle, h is the slab thickness, η its viscosity, $\Delta\rho$ the density contrast between the slab and the mantle, g the gravity acceleration and r the radius of curvature of the slab. Our reference slab is characterized by h of 0.012 m, η_l of 2×10^5 Pa s, $\Delta\rho$ of 100 kg m^{-3}, r of 0.045 m and subducts in a mantle with a thickness H = 0.11 m. The obtained relative characteristic time is equal to 8 min. Finally, the length dimension expressed in the trench motion, plate motion, and amount of subduction can be normalized by the initial length of slab bearing plate, i.e., 0.4 m.

4. Results

[28] Thirty-one out of 60 experiments (Table 2) have been selected to test the influence of (1) plate thickness, (2) plate viscosity, (3) plate width, and (4) mantle thickness. We identify three different possible modes of subduction as a function of the motion of the trench with respect to the box

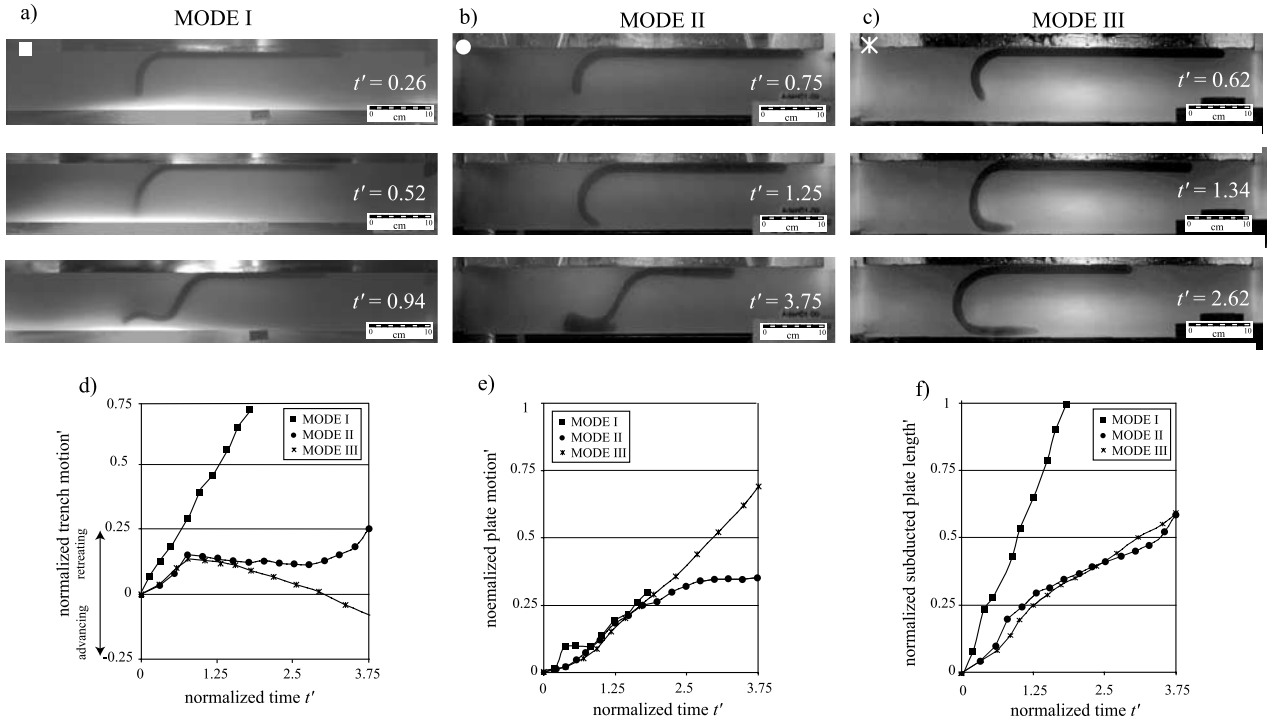

Figure 3. Lateral view of three stages of evolution of experiments characterized by different modes of subduction: (a) mode I, retreating trench mode; (b) mode II, retreating trench mode following an advancing stage; and (c) mode III, advancing trench mode. (d) Normalized trench motion measured in the three experiments presented versus normalized time. (e) Normalized plate motion versus normalized time. (f) Normalized subducted plate length versus normalized time.

reference frame: retreating trench mode (mode I), retreating trench mode following an advancing stage (mode II), and advancing trench mode (mode III).

[29] All the experiments show a typical sequence of three phases: (1) sinking of the slab through the upper mantle, (2) transient slab/lower boundary interaction, and (3) steady state subduction. The experiments share a common behavior during the first phase. Conversely, during the second and the third phases, experiments show different behaviors as a function of their geometrical and rheological parameters. Below, we describe these three phases for experiments equivalent to a lithospheric thickness of 70 km (0.012 m in the model) and to a mantle thickness of 660 km (0.11 m in the model). In the following sections, velocities (of subduction, plate and trench) were calculated from the slope of the curves of Figures 3–7.

4.1. Simple Retreating Mode (Mode I)

[30] The first phase, characterized by the sinking of the slab into the upper mantle, has been already described in detail in previous papers [*Becker et al.*, 1999; *Faccenna et al.*, 2001; *Funiciello et al.*, 2003]. To start subduction, the leading edge of the lithosphere is forced inside the mantle with a shallow dipping angle to obtain enough slab pull able to overcome the resistance at trench. After initiation, the slab sinks into the mantle, the trench retreats, and the slab increases its dip reaching 90° (Figure 3a). The subduction velocity (Figure 3f) increases linearly with the slab length. This process is always associated with a significant displacement of the mantle from beneath the slab driven by the subducting plate [*Funiciello et al.*, 2003]. After about a normalized time of 0.5, the slab reaches the bottom of the mantle (Figure 3a). In the second phase the amount of subduction slows down for few hundredths of normalized time (Figure 3f) while the tip of the slab folds and deforms at depth doubling the bending resistance. From this moment, the flow of the mantle beneath the slab is inhibited by the impermeable barrier and attains a significant lateral out-of-plane component [*Funiciello et al.*, 2003]. The process restarts in the third phase: the trench retreat, the plate motion and the amount of subduction are quite constant from this time (Figures 3d, 3e, and 3f) and the slab dip reaches steady state values of about 60° (Figures 3a–3c), while its tip lies horizontally on the top of the lower mantle. The amount of plate motion (Figure 3e) and trench motion (Figure 3d) are approximately the same as before the phase 2 and their normalized velocities are around 0.3 and 0.4, respectively. The subduction velocity is around 0.7 (Figure 3f).

4.2. Retreating Mode Following an Advancing Stage (Mode II)

[31] As in the simple retreating mode, the subduction starts by increasing trench retreat and subduction velocity (Figures 3b, 3d, and 3f). These two amounts are, however, lower than in the previous mode. The amount of plate motion is also lower (Figure 3e).

[32] The trend of subduction changes drastically when the slab interacts with the 660 km discontinuity, at a normalized time of 0.8. During the second phase, the trench starts to advance at a very low velocity (Figure 3d). Hence the slab assumes a reclined U-shape characterized by an average dip

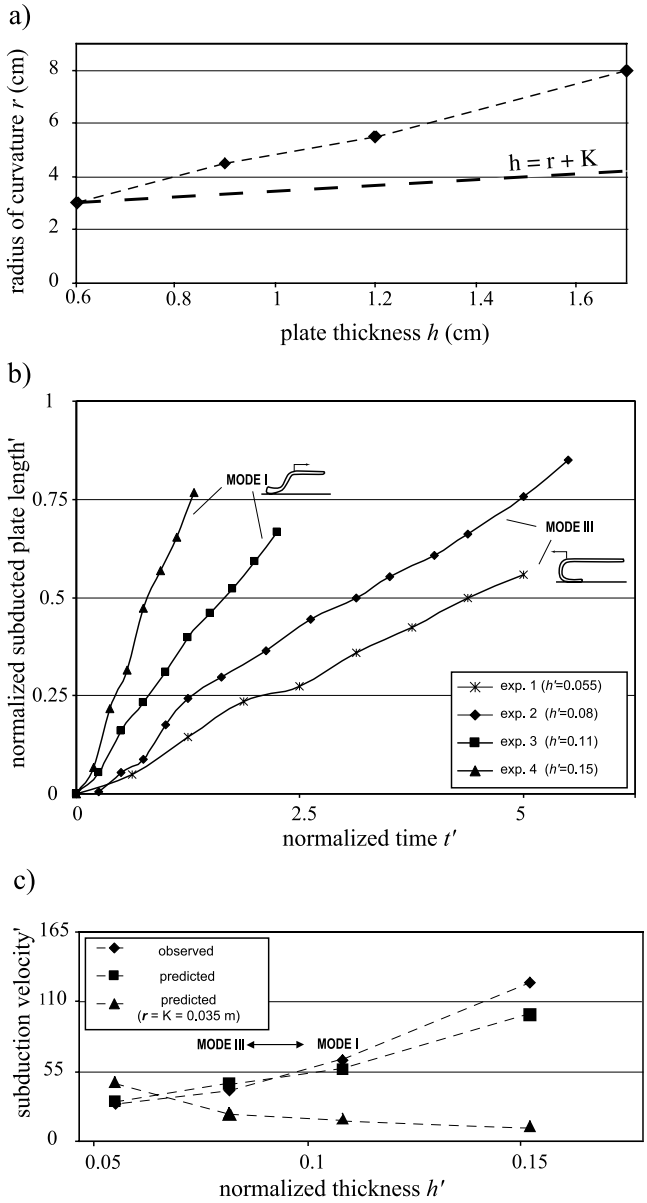

Figure 4. Influence of the plate thickness. (a) Diagram showing radius of curvature r versus plate thickness h measured on the experiments 1, 2, 3, and 4. The dashed line ($h = r + K$) shows that the radius of curvature increases faster the plate thickness. (b) Normalized subducted plate length versus normalized time. At high plate thicknesses the subduction velocity is high, and the trench is retreating (mode I). At low plate thicknesses the subduction velocity is low, and the trench advances (mode III). See text. (c) Normalized subduction velocity versus normalized thickness. The observed velocity of subduction is increasing with plate thickness. The predicted velocity is decreasing with plate thickness when using a constant radius of curvature (equal to 0.035 m corresponding to about 200 km in nature), while it is increasing when using the varying radius as observed in Figure 4a.

of about 90° (Figure 3b). During this phase, the plate velocity is very similar to the mode I during its third phase, around 0.3 (Figure 3e). The normalized velocity of subduction is lower than in the previous mode, around 0.1 (Figure 3f).

[33] At around a normalized time of 2.5, the third phase occurs. The slab tip is folded again for the third time (Figure 3b). From this time, the dip of the slab stabilizes around 60° and trench restarts to retreat at a constant normalized velocity of around 0.3 (Figure 3d). The velocity of subduction stabilizes around a normalized value of about 0.35 (Figure 3f). The plate motion slows down to a low normalized velocity of about 0.05 (Figure 3e).

4.3. Advancing Mode (Mode III)

[34] The first two phases are similar to what already described in the retreating mode II (compare Figures 3b, 3c, and 3d–3f). Actually, the third phase is the continuation of the second one, the trench advances at a roughly constant normalized velocity of 0.1 (Figure 3d), while the average dip of the slab remains constant at around 85° and the normalized plate velocity is constant at about 0.3 (Figure 3e), a value similar to mode I. The subduction velocity is low around 0.2 (Figure 3f).

[35] To sum up, during the steady state phase (third phase), the mode I experiment shows high subduction, plate, and retreating trench velocities. The mode II experiment shows high subduction and retreating trench velocities while the plate velocity is low. Mode III experiment shows a lower subduction velocity, a high plate velocity and a high advancing trench velocity.

4.4. Role of Plate Thickness

[36] Plate thickness (Figure 4) is considered to be an important factor as, in equation (1), it should slow down the subduction velocity [*Conrad and Hager*, 1999]. We here show a set of experiments changing the plate thickness, h, from 0.006 m to 0.017 m (Table 2). The other parameters are kept constant: plate viscosity is set at 3.6×10^5 Pa s, the density contrast between the plate and the mantle at 100 kg cm^{-3}, the width of the plate at 0.1 m and mantle thickness at 0.11 m (Table 2).

[37] We first observed that the radius of curvature is a function of the plate thickness. Its value, measured during the third steady state phase, increases with the thickness of the lithosphere (Figure 4a). We also observed that by varying the plate thickness, the mode of subduction changes. Mode I of subduction typifies the system characterized by thick plate (experiment 4, $h' = 0.15$; Figure 4b). Under this condition the process is particularly fast. The slab reaches the bottom of the box after a t' of only 0.375. In this kind of configuration, where slab pull force is important, the retreating mode is favored. Decreasing the plate thickness (experiment 3, $h' = 0.11$; Figure 4b), the general behavior of the system is similar to that of experiment 4 but the process is slower. The first phase becomes longer and the steady state dimensionless subduction velocity, v', is lower. At low plate thickness (experiment 1, $h' = 0.05$; experiment 2, $h' = 0.08$; Figure 4b), the subduction velocity is slowed down in a more significant way. The first phase ends after a dimensionless time of 1.8 while the subduction attains the steady state behavior only after a dimensionless

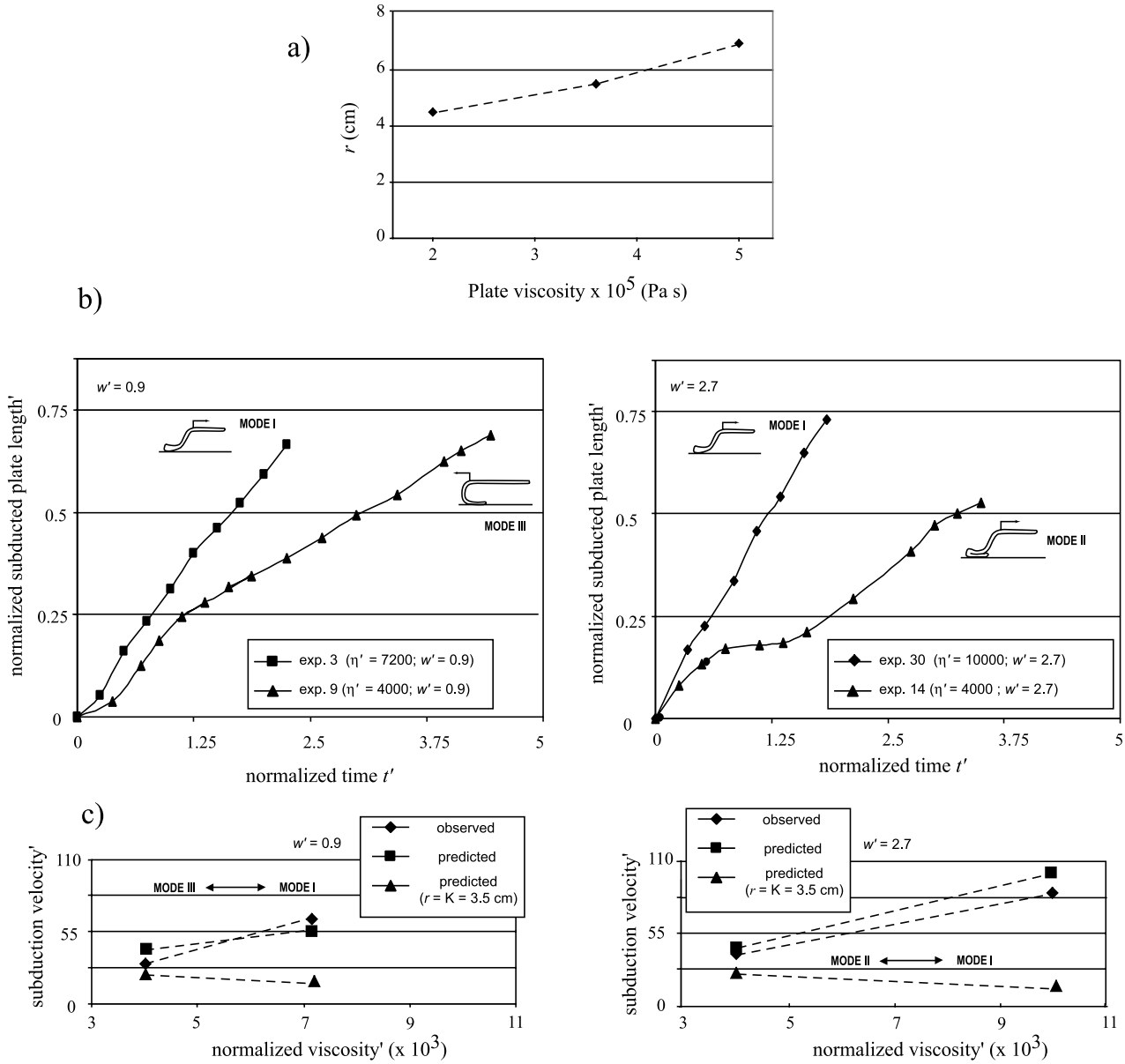

Figure 5. Influence of the plate viscosity. (a) Measured radius of curvature versus plate viscosity. We observe that the radius of curvature increases with the plate viscosity. (b) Normalized subducted plate length versus normalized time. (left) For a normalized plate width of 0.9, the velocity is higher when the viscosity is higher. (right) The same result is found for a plate width of 2.7. (c) Normalized subduction velocity versus normalized viscosity. We found that the velocity increases with the viscosity, the result obtained in predictions when the observed radius of curvature is taken into account. When the radius is taken constant, a decrease is obtained.

time of 3.1. Moreover, the velocity is lower than in the high plate thickness experiments. In this kind of configuration, the advancing style (mode III) is favored.

[38] The analysis of the velocity of subduction during the third phase of the entire set of experiments thus shows an increase with the increase of plate thickness (Figure 4c). The increasing slab pull force can explain this behavior. Additionally, we found that the radius of curvature increases linearly with the thickness of the plate (Figure 4a). Moreover, the radius of curvature increases faster than the plate thickness (Figure 4a, dashed line). Thus increasing the plate thickness actually implies a decrease of the viscous dissipation due to the plate bending (as it is proportional to h/r, equation (3)). If the radius of curvature was assumed constant, as by *Conrad and Hager* [1999], we would have obtained the opposite behavior (Figure 4c).

[39] Finally, we observe that, while the advancing experiments (mode III) show a good agreement between predicted and observed velocity, the retreating experiments (modes I and II) run slightly faster than predicted (Figure 4c).

4.5. Role of Plate Viscosity

[40] The plate viscosity (Figure 5) is supposed to play a fundamental role in the system, as it should slow down

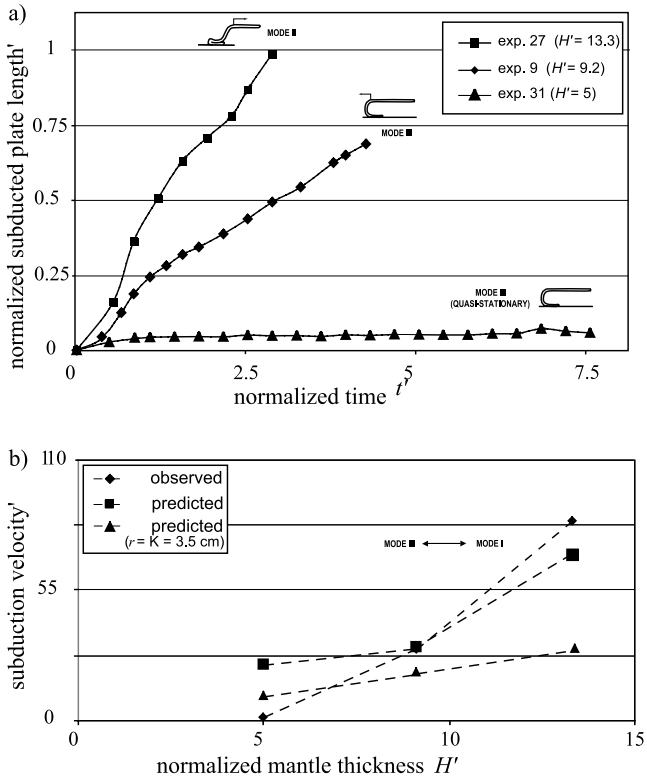

Figure 6. Influence of the mantle thickness. (a) Normalized subducted plate length versus normalized time. For a high mantle thickness the amount of subduction is very high, and a mode II is observed. For a lower mantle thickness the amount of subduction is lower, and a mode III is observed. For a very low mantle thickness a quasi-stationary subduction is observed. (b) Normalized subduction velocity versus normalized mantle thickness. The observed velocity increases with the mantle thickness. This behavior is also predicted in the analytical solution.

the velocity of subduction due to the increasing resistance of the slab to bending at the trench (equation (1) and *Conrad and Hager* [1999] and *Becker et al.* [1999]). We ran a set of experiments using subducting plate viscosities ranging between 2 and 5×10^5 Pa s (Table 2). The other parameters were kept constant: the density contrast between the plate and the honey was set at 100 kg m^{-3}, plate thickness at 0.012 m, plate width at 0.1 m and 0.3 m and mantle thickness at 0.11 m. First, we found that the radius of curvature depends on the viscosity, increasing quite linearly from 0.045 to about 0.07 m (Figure 5a).

[41] Experiments at 0.1 m width show different behaviors depending on the plate viscosity. With a high-viscosity plate, the trench retreats (mode I; Figure 5b, left), whereas at low viscosity it advances (mode III; Figure 5b, left). For a 0.3 m width plate, the plate always shows a retreating trench style of subduction: mode I at high viscosity and mode II at low viscosity (Figure 5b, right).

[42] The observed velocity of subduction increases with the viscosity (Figures 5b and 5c). The predicted velocity depends upon the radius of curvature (Figure 5c). For a constant radius of curvature the velocity of subduction is expected to decrease with the viscosity, because (h/r) is constant. Inserting the real radius of curvature value, conversely, the velocity increases following a trend that is similar to what observed. This somehow confirms the validity of the analytical solution to predict the velocity of subduction (equation (1)). The increase of viscosity is counterbalanced by the decrease of (h/r) (Figure 5a).

4.6. Role of Mantle Thickness

[43] In natural systems the depth reached by the slab as imaged by velocity anomalies can be strongly different [*Fukao et al.*, 2001]. The length of the slab is considered to be important ingredient controlling the subduction. An increase of the length of the subducted lithosphere increases the slab pull force and vice versa [*Lithgow-Bertelloni and Richards*, 1998]. We then changed the thickness of the mantle (Figure 6) varying the depth of the box from 0.06, to 0.11 and to 0.16 m (Table 2). The other parameters are kept constant: plate thickness is set at 0.012 m, plate width at 0.1 m, plate viscosity at 2×10^5 Pa s, the density contrast between the plate and the mantle at 100 kg m^{-3}. The results of the experiments (Figure 6a) show that for average mantle thickness the trench tends to advance (experiment 9, mode III, as seen before experiment of Figure 5b). For the case of low mantle thickness no real subduction occurred and after an initial phase of advancing, subduction stops, whereas with high mantle thickness the trench retreats (mode II, Figure 6a).

[44] The observed and predicted velocity of subduction both increase with increasing mantle thickness, which is mainly related to the increase of slab pull.

4.7. Role of Plate Width

[45] The role of the width of the plate is varied investigated varying the width from 0.05 to 0.6 m (Figure 7). Different configurations have been tested, changing the thickness of the mantle, plate viscosity and thickness (Table 2). In a first set ("A," Figures 7a and 7b), the mantle thickness is 0.11 m, the plate thickness and viscosity are of 0.012 m and 2×10^5 Pa s, respectively. In a second set ("B," Figures 7c and 7d), the mantle thickness is 0.11 m, the plate thickness and viscosity are of 0.009 m and 3.6×10^5 Pa s, respectively. In a third set ("C," Figures 7e and 7f), the mantle thickness is 0.11 m, the plate thickness and viscosity are of 0.006 m and 3.6×10^5 Pa s, respectively. In the forth set ("D," Figures 7g and 7h), the mantle thickness is 0.11 m, the plate thickness and viscosity are of 0.012 cm and 0.9×10^5 Pa s, respectively, and the density contrast is 150 kg m^{-3} instead of 100 kg m^{-3}. In the fifth set ("E," Figures 7i–7j), the mantle thickness is 0.16 m, the plate thickness and viscosity are of 0.012 m and 2×10^5 Pa s, respectively.

[46] Each group of experiments shows either an advancing (mode III) or a retreating behavior (modes I and II). The only exception is represented by the experiments of group "A" (Figures 7a and 7b), which shows both behaviors (modes II and III). In particular, we observe that plates with smaller widths tend to have an advancing trend while larger ones tend to have a retreating trend. For the other cases, we find that both high mantle thickness experiments and high-density ones show a tendency to have retreating behavior (modes I and II) (Figures 7g and 7i).

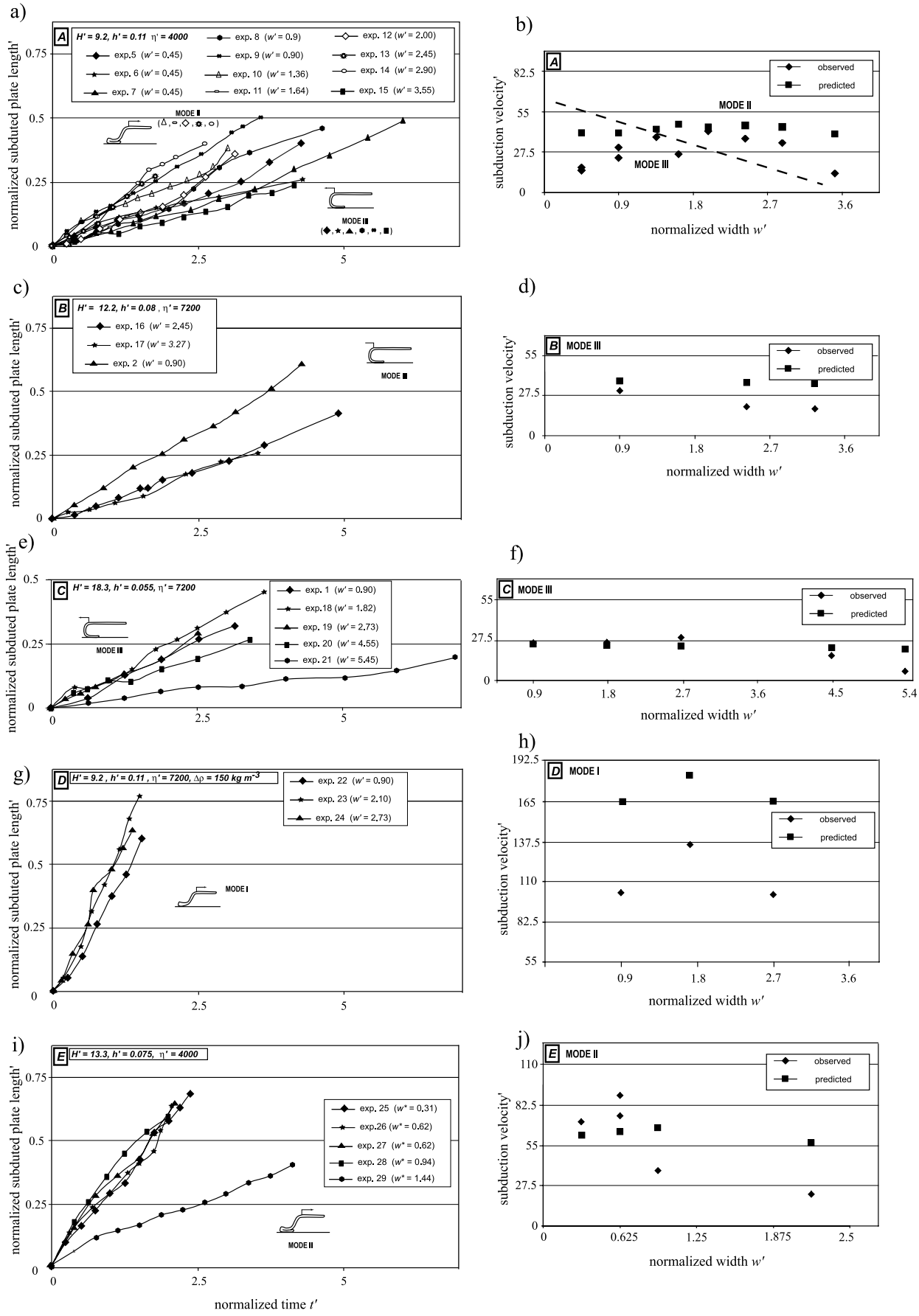
a)
A H' = 9.2, h' = 0.11 η' = 4000
exp.5 (w' = 0.45)
exp. 6 (w' = 0.45)
exp. 7 (w' = 0.45)
exp. 8 (w' = 0.9)
exp. 9 (w' = 0.90)
exp. 10 (w' = 1.36)
exp. 11 (w' = 1.64)
exp. 12 (w' = 2.00)
exp. 13 (w' = 2.45)
exp. 14 (w' = 2.90)
exp. 15 (w' = 3.55)
MODE I
MODE II
normalized subduted plate length'
b)
A
observed
predicted
MODE II
MODE III
subduction velocity'
normalized width w'
c)
B H' = 12.2, h' = 0.08 , η' = 7200
exp. 16 (w' = 2.45)
exp. 17 (w' = 3.27)
exp. 2 (w' = 0.90)
MODE I
d)
B MODE III
observed
predicted
e)
C H' = 18.3, h' = 0.055, η' = 7200
exp. 1 (w' = 0.90)
exp.18 (w' = 1.82)
exp. 19 (w' = 2.73)
exp. 20 (w' = 4.55)
exp. 21 (w' = 5.45)
MODE II
f)
C MODE III
observed
predicted
g)
D H' = 9.2 , h' = 0.11 , η' = 7200, Δρ = 150 kg m-3
exp. 22 (w' = 0.90)
exp. 23 (w' = 2.10)
exp. 24 (w' = 2.73)
MODE I
h)
D MODE I
observed
predicted
i)
E H' = 13.3, h' = 0.075, η' = 4000
exp. 25 (w* = 0.31)
exp.26 (w* = 0.62)
exp. 27 (w* = 0.62)
exp. 28 (w* = 0.94)
exp. 29 (w* = 1.44)
MODE II
normalized time t'
j)
E MODE II
observed
predicted

Figure 7

[47] The increasing width of the plate, however, generally causes a slow down of the subduction velocity (Figures 7b, 7d, 7f, 7h, and 7j). The tendency for the subduction velocity to slow down with increasing plate width was expected since it is predicted by equations (1) and (6) (Figures 7b, 7d, 7f, 7h, and 7j). The mantle contribution is calculated following *Conrad and Hager* [1999] by assuming that the size of the plate is proportional to the square root of the product of length and plate width. Result of the experiment shown in Figure 2 shows, however, that the viscous coupling is low as the viscosity of the mantle is. Therefore it is possible that the decrease in the subduction velocity, rather pronounced for the case of large plate, is mostly due to the overpressure related to mantle circulation during the motion of the slab inside the mantle [*Funiciello et al.*, 2003, 2004]. This can explain the departure of the predicted value from the expect one. In the same manner, we interpret the tendency of large plate to retreat observed in experiments of Figure 7b, as due to plate/slab interaction. This change, however, has been observed only in this set of experiments, probably because the system is near the partition between retreat and advancing modes.

5. Interpretation of the Experimental Results

[48] In the experimental program presented here, we have tested four parameters that can influence the style of subduction: the plate viscosity, the plate thickness and width, and the mantle thickness. We identify three different modes of subduction, characterized by a different partitioning of the subduction velocity between plate and trench velocity (Figure 3): a ''retreating'' mode (mode I), ''advancing followed by a retreating'' mode (mode II), ''advancing'' mode (mode III). All the experiments share a common behavior during the initial phase, when slab dives into the upper mantle (phase I): the trench retreats and the velocity of subduction increases increasing the length of subducted material. The different style of subduction is already distinctive when the slab reaches the deep discontinuity (phase II), that is before arriving at a steady state behavior (phase III). Mode I (Figures 3a and 3d–3f) shows that subduction slows down shortly during interaction between the slab and the deep discontinuity and then regains its faster rate in a steady state configuration, where slab attains a shallow dip and the trench retreat faster. Mode II (Figures 3b and 3d–3f) is a mixed mode as the slab shows a short advancing phase II before reaching the third steady state retreating phase, with a velocity field similar to though slower than mode I. Mode III (Figures 3c–3f) shows a backward reclined advancing slab with a velocity of subduction comparable to mode II but producing a higher plate.

[49] Two questions arise from our results: can we predict the subduction velocity and, consequently, the way forces are balanced in the experiments? Can we predict the mode of subduction and, consequently, the velocity of the plate?

[50] To answer to the first question, we adopt the *Conrad and Hager* [1999] formulation for the velocity of subduction (equation (1)) adapted to our case (3-D convection and subduction). Figure 8a shows that predicted velocity from equation (1) properly approximates the observed velocity if the real radius of curvature is inserted independently of the mode of subduction.

[51] We observed that the radius of curvature plays an important role in the system [*Becker et al.*, 1999; *Conrad and Hager*, 1999] that depends upon the viscosity and the thickness of the slab (Figure 4a and 6a). For example, a stiffer slab does not produce a slowing down of the system because there is an increase in radius of curvature (Figure 6c). This result points out that the assumption of a constant radius of curvature that is independent from the plate parameter [*Conrad and Hager*, 1999] cannot be adopted. In general terms, our experimental results confirm the finding that bending resistance does represent by far the largest contribution in the system [*Becker et al.*, 1999; *Conrad and Hager*, 1999; *Funiciello et al.*, 2003]. The other resisting force is represented by slab-mantle interaction. This has a twofold effect. The first is related to the viscous shear. In our setup this contribution is very low (Figure 2) due to the high slab/mantle viscosity ratio. The other is related to local overpressure due to the lateral motion of the slab that forces the mantle material to flow around the slab edges. This force indeed can play an important role, as increasing the width by a factor of five produce a reduction of the subduction velocity by a factor of about two and, under peculiar circumstances, can also influence the mode of subduction. The role of this contribution has been previously tested by *Funiciello et al.* [2004] changing systematically the lateral boundary conditions of the system.

[52] Summing up, we estimated that the bending resistance represents the most important resisting contribution ranging from 75% to 95% of the total resisting forces (Figure 8b). The slab-mantle contribution represents the remaining part ranging from 5% to 25% (Figure 8b). *Schellart* [2004], using the same experimental setup, has measured the deformation of markers placed inside the slab during the first phase of subduction concluding that bending resistance is limited to 15–30%, while the rest is mostly related to the rollback-induced mantle flow. It is our opinion that this discrepancy can be related to the lower slab/mantle viscosity ratio and to the accuracy in determining the force in the experiment (+30% [*Schellart*, 2004]).

[53] Answering the second question concerning the possibility of predicting the mode of subduction and, in turn,

Figure 7. Influence of plate width. (a) (c), (e), (g), (i) Normalized subducted plate length versus normalized time for different plate widths. Five sets of experiments (A, B, C, D, E) are presented varying parameters such as viscosity, thickness, and density of the plate and thickness of the mantle. In each set the experiments display the same trench behavior (mode I, II, or III) except for set A, where both the modes II and III are observed. See text. (b), (d), (f), (h), (j) Normalized subduction velocity versus normalized width for the five set of experiments (A, B, C, D, E). The observed and predicted velocities are compared. A general trend of decrease of the velocity increasing the width of the plate is observed. In Figure 7b the dashed line separates two fields with different styles of subduction.

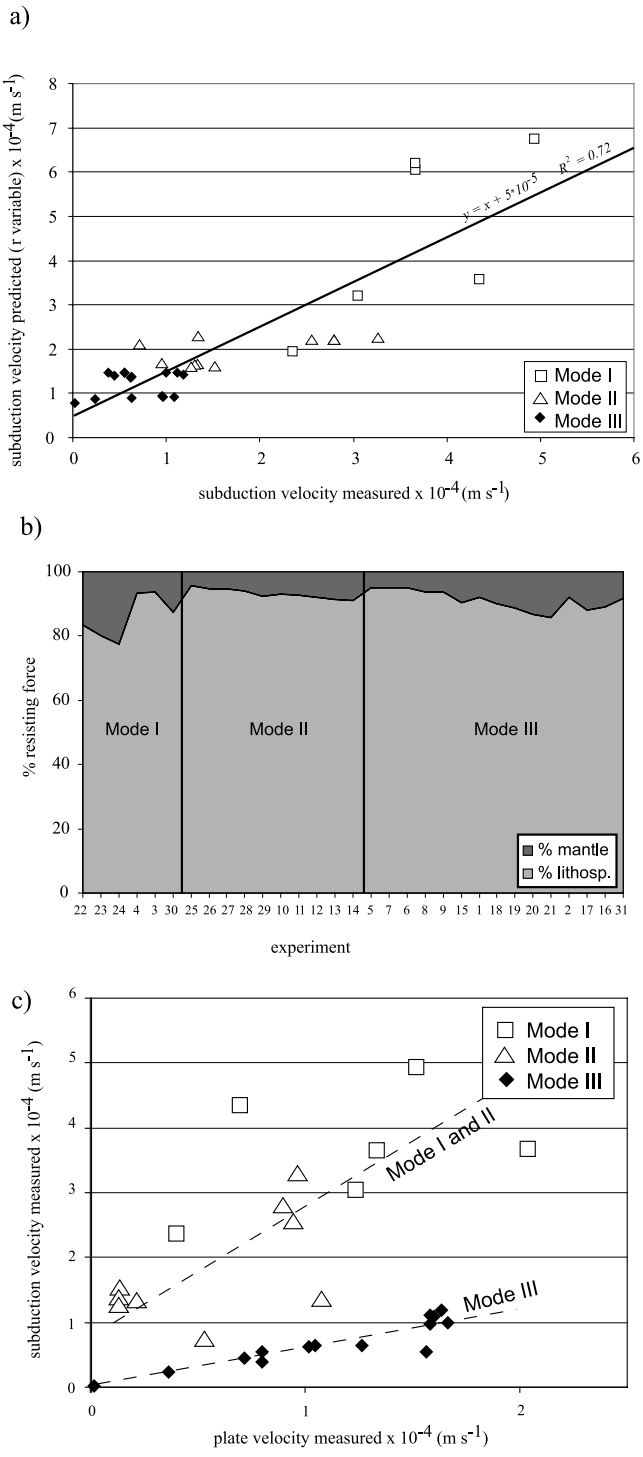

Figure 8. (a) Predicted subduction velocity versus measured subduction velocity. The predicted velocity is calculated using equation (1) and the radius of curvature observed in the experiments. The analytical solution gives a good estimation of the subduction velocity, as attested by the linear regression whose slope is one and correlation coefficient is good. (b) Contribution of the resisting forces in the experiments. The bending resistance generally composes between 75% and 95% of the resisting forces. (c) Measured subduction velocity versus measured plate velocity.

the plate velocity, is not trivial as the velocity of the plate is a direct consequence of the mode of subduction. Figure 8c shows that both for the retreating and for the advancing mode of subduction the velocity of the plate depends directly on the velocity of subduction. That is, in mode III, the velocity of the plate is higher (about 30%) than the velocity of subduction, as the trench advances, whereas in the retreating mode, the speed of the plate is much lower than that of subduction (about 3 times lower), which in this case is accommodated by the retreat of the trench.

[54] Summing up, it is impossible to predict a priori the plate velocity only from the velocity of subduction, but one should consider the way the trench moves. Our experimental results show that the radius of curvature, which depends upon the plate characteristics (stiffness and thickness) and the mantle thickness, does exert a primary control on the trench behavior. For the case of a retreating trench, one can assume that the plate motion is only a fraction of the subduction velocity whereas for the case of an advancing trench the velocity of the plate is higher than that of subduction. Under specific range of parameters, a small change in the radius of curvature produces a change in the style of subduction and a consequent different partitioning of the amount of subduction velocity into plate and trench velocity. Moving from the retreating to the advancing field, for example, can produce an increase in the plate speed of about five times while preserving the same subduction velocity.

[55] In general terms, the three modes depend upon the distribution of the forces active into the system. If the slab pull force is very high, as for example for the case of high mantle thickness (Figure 7), the system is more prone to retreat (modes I and II).

[56] Considering the importance of bending in the force equilibrium, we try to express the subduction velocity in terms of radius of curvature normalized versus the mantle thickness (Figure 9). It is possible to distinguish three different fields.

[57] 1. For small mantle thickness (corresponding to about 300 km in nature), r/H is larger than 0.8 and subduction does not occur. The resisting force related to plate bending in this case is too large compared to the small amount of subducted material.

[58] 2. For large mantle thickness (corresponding to about 1000 km in nature), r/H is lower than 0.4 and the style of subduction follows mode II. Subduction velocity, in this case, varies independently from the radius of curvature.

[59] 3. For a mantle thickness scaled for the upper mantle (660 km), r/H is between 0.3 and 0.8 and the velocity and the style of subduction depend upon the radius of curvature. In particular, we observe that the style of subduction changes from a mode I when r/H is between 0.5 and 0.8, to mode II, for r/H between 0.4 and 0.5 and mode III, when r/H is equal or lower than 0.4. Around 0.4, we also found a dependency on the width of the plate (Figure 5). In this peculiar range, in fact, we can pass from mode II to mode III when the width of the plate gets smaller than the mantle thickness. We infer that this is due mostly to the motion of mantle material around the slab edge. Mostly in the retreating configuration [*Funiciello et al.*, 2003, 2004], in fact, the motion of the slab induces the displacement of the mantle from below the slab. It is possible that only in this crucial

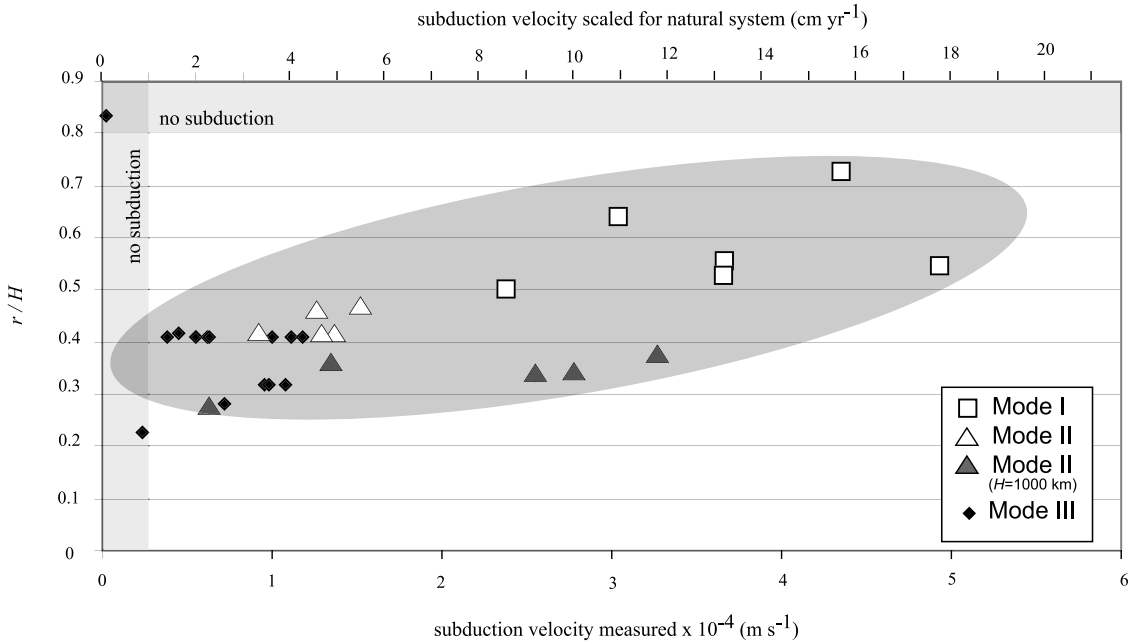

Figure 9. Radius of curvature normalized for the mantle thickness versus the velocity of subduction measured in the experiment and scaled to nature. The mode of subduction depends on the ratio: radius of curvature/mantle thickness. For ratio higher than 0.5 the mode I prevails and the subduction velocity is high. For ratio between 0.4 and 0.5 the mode II prevails, and the velocity of subduction is lower. For ratio less than or equal to 0.4, mode III is found, and the subduction velocity is low. At 0.4 the behavior is complex and depends also on the width of the plate.

range (r/H about 0.4) is the work done for the flow to turn around the plate such that the retreating configuration is not favored. Further experiments are needed to quantify this process.

[60] Finally, we did not test the role of mantle viscosity. Further experiments are in progress to quantify the role of this parameter.

6. Insights Into Natural Systems

[61] Experimental results are difficult to export to a natural system. This is because of the lack of a proper scaling for temperature-dependent viscosity and because trench kinematics can be influenced by the upper plate motion, which is not modeled here. Despite these oversimplifications, however, is it tempting to look where Earth parameters distribute in the diagram presented in Figure 9. The radius of curvature, r, estimated from the Wadati-Benioff zones, mostly ranges from 200 and 400 km, with a peak at 280 km a mean at 380 km [*Heuret and Lallemand, in press*]. The value H is more difficult to estimate. Tomographic images confirm that the shut down of seismicity at a depth corresponding to the 660 km discontinuity can be related to a lost in the integrity of slab and locate large mass anomalies stagnating over the transition zone [*Isacks and Molnar*, 1971]. However, it has been generally accepted that subducting material can descend to depth greater than 660 km [*van der Hilst et al.*, 1991]. Nevertheless the effective possibility for this deep material to transmit stress to the attached plate is weakened by the fact that this material would not be directly connected with the shallower material and, while descending into the deeper mantle layer, it would be supported by viscous shear stresses [*Conrad and Lithgow-Bertelloni*, 2002]. Below 660 km depth, the concurrent action of the possible increase in viscosity (order of 30–100 [*Hager*, 1984; *Forte and Mitrovica*, 1996; *Mitrovica and Forte*, 1997]) and endothermic phase change [*Christensen and Yuen*, 1984; *Tackley et al.*, 1993; *Pysklywec and Mitrovica*, 1998] could effectively retard slab penetration in the lower mantle. It is thus reasonable to believe that the fragmentation of the slab, well recognized both for advancing trenches as the Himalayas and for retreating ones (see, e.g., the Tyrrhenian or the Izu-Bonin) at a depth of about 660 km, would limit the amount of material that effectively drives the slab pull to portion that lies in the upper mantle. The ratio between r/H on the Earth should be in the range between 0.3 and 0.6 with a peak at 0.4. In this range the Earth system is placed in the critical range where the subduction style can easily skip from "advancing" (mode III) to "retreating" (modes I and II). Hence it is possible that a small perturbation of the lithospheric rigidity would produce a large impact on the plate tectonic style. For example, entrance at a trench of a more buoyant thick aseismic ridges would produce an increase in the radius of curvature, a decrease in the slab dip, an increase in the retreat velocity and a decrease in the plate velocity. Or the other way around, efficient serpentinization of the oceanic crust could effectively decrease the plate strength and, consequently, the radius of curvature favoring the speed up of the plate. It is interesting to recall that a change in style of subduction does not cause a dramatic change in the subduction velocity but the velocity of the plate can change by about five times. In addition, under these peculiar conditions, variations of the width of

the plate could produce a change in the mode of subduction. In particular, we have observed that when plate width is equal to or less than the mantle thickness, plates are more prone to advance. This also means that the fragmentation of a large plate into smaller plates perpendicular to the trenches should produce plates that will advance faster. This mechanism could eventually contribute explaining the problem of Gondwana breakup where some of the plates, such as greater India, speed up to 16 cm yr^{-1} northward [*Patriat and Achache*, 1984; *Besse and Courtillot*, 1988] soon after the breakup and the decrease of their size (and especially their width).

[62] Our results suggest that the Earth system is in a crucial equilibrium for the interplay between the rigidity of the plate and the stratification of the mantle. The plate tectonic style both reconstructed and actually observed shows a huge variety of configurations with episodes of indentation (advancing) and episodes of back-arc extension (retreating). This rather unique setting should be then responsible for the complexity of tectonic styles we observe on Earth: changing the temperature or gravity field of the planet one should then expect a departure from the Earth plate tectonic style. One can speculate, for example, that in a colder Earth oceanic plates get thicker. This mechanism could, in principle, cause the speed up of the plate as the radius of curvature increases as the slab pull force does. Our experiments, however, point out that this process should arrive to a threshold in which subduction stops, as if the radius of curvature increases too much with respect to the mantle thickness. Our data set show that if the mantle thickness remains constant, the maximum thickness for an oceanic plate to subduct is in the order of 120–140 km. This limiting factor is something already predicted by *Conrad and Hager* [1999] assuming a constant radius of curvature. This prediction can be maybe relevant implication for other planet as for Mars. On the other hand, we can predict that in a hotter Earth plate would lead to a thinner plate, that is, a smaller radius of curvature, which in turn would cause a slow subduction velocity. One can then imagine that the change of the plate thickness during the Earth history would have big impact on the way the plate tectonics worked. In the early stage of the Earth, one should expect that plate tectonics started slowly and accelerating while temperature is dissipated by convection up to the point where plate gets too thick and unable to deform and subduct into the mantle.

7. Conclusions

[63] The results of the laboratory experiments indicate that the style of subduction, the motion of the trench and of the plate are controlled by the way the plate bends inside the mantle and this depends upon its stiffness, its velocity but also on the depth of the mantle [*Ribe*, 2003]. In addition, in contrast with previous approximations [*Conrad and Hager*, 1999], we have found a linear dependency of the lithospheric radius of bending from the viscosity of the plate and its thickness. This reduces the possibility that the mantle contribution could play an important role in controlling the subduction velocity if lithospheric viscosity is higher than the upper mantle viscosity. Moreover, it strongly restricts the possibility of having an accurate evaluation of the subduction velocity assuming a constant radius of curvature.

[64] Our results suggest also that the Earth system is in a crucial equilibrium for the interplay between the rigidity of the plate and the stratification of the mantle. This rather unique setting should be then responsible for the complexity of tectonic styles we observe on Earth.

[65] **Acknowledgments.** Experiments have been performed at the Laboratory of Experimental Tectonics of University of Roma TRE. Discussions with Thorsten Becker and with Domenico Giardini improved the quality of the final work. We thank Clint Conrad for its careful review as well as an anonymous associate editor who improved and clarified the early version of the manuscript.

References

Becker, T., and R. O'Connell (2001), Predicting plate velocities with mantle circulation models, *Geochem. Geophys. Geosyst.*, *2*, doi:10.1029/2001GC000171.

Becker, T., C. Faccenna, D. Giardini, and R. O'Connell (1999), The development of slabs in the upper mantle: Insights from numerical and laboratory experiments, *J. Geophys. Res.*, *104*, 15,207–15,226.

Besse, J., and V. Courtillot (1988), Paleogeographic maps of the Indian ocean bordering continents since the upper Jurassic, *J. Geophys. Res.*, *94*, 2787–2838.

Brace, W. F., and D. L. Kohlstedt (1980), Limits on lithospheric stress imposed by laboratory experiments, *J. Geophys. Res.*, *85*, 6248–6252.

Bunge, H. P., M. A. Richards, D. C. Engebretson, and J. R. Baumgardner (1997), A sensitivity study of three-dimensional spherical mantle convection at 108 Rayleigh number: Effects of depth-dependent viscosity, heating mode, and endothermic phase change, *J. Geophys. Res.*, *102*, 11,991–12,007.

Chapple, W. M., and T. E. Tullis (1977), Evaluation of the forces that drive the plates, *J. Geophys. Res.*, *82*, 1967–1984.

Christensen, U. R. (1996), The influence of trench migration on slab penetration into the lower mantle, *Earth Planet. Sci. Lett.*, *140*, 27–39.

Christensen, U. R., and D. Yuen (1984), The interaction of the subducting lithospheric slab with a chemical or phase boundary, *J. Geophys. Res.*, *89*, 4389–4402.

Conrad, C. P., and B. Hager (1999), Effects of plate bending and fault strength at subduction zones on plate dynamics, *J. Geophys. Res.*, *104*, 17,551–17,571.

Conrad, C. P., and C. Lithgow-Bertelloni (2002), How mantle slabs drive plate tectonics, *Science*, *298*, 207–209.

Conrad, C. P., S. Bilek, and C. Lithgow-Bertelloni (2004), Great earthquakes and slab-pull: Interaction between seismic coupling and plate-slab coupling, *Earth Planet. Sci. Lett.*, *218*, 109–122.

Davies, G. F. (1995), Penetration of plates and plumes through the mantle transition zone, *Earth Planet. Sci. Lett.*, *133*, 507–516.

Davies, G. F., and M. A. Richards (1992), Mantle convection, *J. Geol.*, *100*(2), 151–206.

Faccenna, C., P. Davy, J.-P. Brun, R. Funiciello, D. Giardini, M. Mattei, and T. Nalpas (1996), The dynamics of back-arc extensions: An experimental approach to the opening of the Tyrrhenian sea, *Geophys. J. Int.*, *126*, 781–795.

Faccenna, C., D. Giardini, P. Davy, and A. Argentieri (1999), Initiation of subduction at Atlantic-type margin: Insight from laboratory experiments, *J. Geophys. Res.*, *104*, 2749–2766.

Faccenna, C., F. Funiciello, D. Giardini, and P. Lucente (2001), Episodic back-arc extension during restricted mantle convection in the central Mediterranean, *Earth Planet. Sci. Lett.*, *187*, 105–116.

Forsyth, D., and S. Uyeda (1975), On the relative importance of the driving forces of plate motion, *Geophys. J. R. Astron. Soc.*, *43*, 163–200.

Forte, A. M., and J. X. Mitrovica (1996), New inferences of mantle viscosity from joint inversion of long-wavelength mantle convection and post glacial rebound data, *Geophys. Res. Lett.*, *23*, 1147–1150.

Fukao, Y., S. Widiyantoro, and M. Obayashi (2001), Stagnant slabs in the upper and lower mantle transition region, *Rev. Geophys.*, *39*, 291–323.

Funiciello, F., C. Faccenna, D. Giardini, and K. Regenauer-Lieb (2003), Dynamics of retreating slabs: 2. Insights from three-dimensional laboratory experiments, *J. Geophys. Res.*, *108*(B4), 2207, doi:10.1029/2001JB000896.

Funiciello, F., C. Faccenna, and D. Giardini (2004), Role of lateral mantle flow in the evolution of subduction systems: Insights from laboratory experiments, *Geophys. J. Int.*, *157*, 1393–1406.

Griffiths, R. W., R. I. Hackney, and R. D. van der Hilst (1995), A laboratory investigation on effects of trench migration on the descent of subducted slab, *Earth Planet. Sci. Lett.*, *133*, 1–17.

Guillou-Frottier, L., J. Buttles, and P. Olson (1995), Laboratory experiments on the structure of subducted lithosphere, *Earth Planet. Sci. Lett.*, *133*, 19–34.

Hager, B. H. (1984), Subducted slab and the geoid: Constraints on mantle rheology and flow, *J. Geophys. Res.*, *89*, 6003–6015.

Hager, B. H., and R. J. O'Connell (1978), Subduction zone dip angles and flow driven by plate motion, *Tectonophysics*, *50*, 111–133.

Heuret, A., and S. Lallemand (2004), Plate motions, slab dynamics and back-arc deformation, *Phys. Earth Planet. Inter.*, in press.

Isacks, B. L., and P. Molnar (1971), Distribution of stresses in descending lithosphere from a global survey of focal mechanism solution of mantle earthquakes, *Rev. Geophys.*, *9*, 103–174.

Kincaid, C., and P. Olson (1987), An experimental study of subduction and slab migration, *J. Geophys. Res.*, *92*, 13,832–13,840.

King, S. D., and B. H. Hager (1990), The relationship between plate velocity and trench viscosity in Newtonian and power-law subduction calculations, *Geophys. Res. Lett.*, *17*, 2409–2412.

Lithgow-Bertelloni, C., and M. A. Richards (1998), The dynamics of Cenozoic and Mesozoic plate motions, *Rev. Geophys.*, *36*, 27–78.

Mitrovica, J. X., and A. M. Forte (1997), Radial profile of mantle viscosity: Results from the joint inversion of convection and postglacial rebound observables, *J. Geophys. Res.*, *102*, 2751–2769.

Patriat, P., and J. Achache (1984), India-Asia collision chronology has implications for crustal shortening and driving mechanisms of plates, *Nature*, *311*, 615–621.

Pysklywec, R. N., and J. X. Mitrovica (1998), Mantle flow mechanisms for the large-scale subsidence of continental interiors, *Geology*, *26*(8), 687–690.

Ranalli, G. (1995), *Rheology of the Earth*, CRC Press, Boca Raton, Fla.

Ribe, N. M. (2003), Periodic folding of viscous sheets, *Phys. Rev. E*, *68*, 036305.

Ricard, Y., C. Doglioni, and R. Sabadini (1993), Differential rotation between lithosphere and mantle: A consequence of lateral mantle viscosity variations, *J. Geophys. Res.*, *96*, 8407–8415.

Schellart, W. P. (2004), Quantifying the net slab pull force as a driving mechanism for plate tectonics, *Geophys. Res. Lett.*, *31*, L07611, doi:10.1029/2004GL019528.

Tackley, P. J., D. J. Stevenson, G. A. Glatzmaier, and G. Schubert (1993), Effects of an endothermic phase transition at 670 km depth in a spherical model of convection in the Earth's mantle, *Nature*, *361*, 699–704.

Tetzlaff, M., and H. Schmeling (2000), The influence of olivine metastability on deep subduction of oceanic lithosphere, *Phys. Earth Planet. Inter.*, *120*, 29–38.

Turcotte, D. J., and R. E. Oxburgh (1967), Finite amplitude convection cells and continental drift, *J. Fluid Mech.*, *28*, 29–41.

Turcotte, D. L., and G. Schubert (1982), *Geodynamics: Application of Continuum Physics to Geological Problems*, 450 pp., John Wiley, Hoboken, N. J.

van der Hilst, R., R. Engdahl, W. Spakman, and G. Nolet (1991), Tomographic imaging of subducted lithosphere below northwest Pacific island arcs, *Nature*, *353*, 37–43.

Weijermars, R., and H. Schmeling (1986), Scaling of Newtonian and non Newtonian fluid dynamics without inertia for quantitative modelling of rock flow due to gravity (including the concept of rheological similarity), *Phys. Earth Planet. Inter.*, *43*, 316–330.

Wortel, R. (1982), Seismicity and rheology of subducted slabs, *Nature*, *296*, 553–556.

Zhong, S., and M. Gurnis (1995), Mantle convection with plates and mobile, faulted margins, *Science*, *266*, 838–843.

N. Bellahsen, Department of Geological and Environmental Sciences, Stanford University, 450 Serra Mall, Building 320, Stanford, CA 94305-2115, USA. (nicolasb@pangea.stanford.edu)

C. Faccenna and F. Funiciello, Dipartimento di Scienze Geologiche, Università degli Studi Roma TRE, L.go S.L. Murialdo 1, I-00146 Rome, Italy.